

Quasielastic $^{12}\text{C}(e, e'p)$ reaction at high momentum transfer

J. H. Morrison,^{*} H. Baghaei,[†] W. Bertozzi, S. Gilad, J. Glickman,[‡] C. E. Hyde-Wright,[§] N. Kalantar-Nayestanaki,^{||}
R. W. Lourie,[¶] S. Penn,^{**} P. E. Ulmer,[§] and L. B. Weinstein[§]

Department of Physics, Massachusetts Institute of Technology, Cambridge, Massachusetts 02139

B. H. Cottman,^{††} L. Ghedira, and E. J. Winhold

Department of Physics, Rensselaer Polytechnic Institute, Troy, New York 12181

J. R. Calarco and J. Wise^{‡‡}

Department of Physics, University of New Hampshire, Durham, New Hampshire 03824

P. Boberg,^{§§} C. C. Chang, and D. Zhang

Department of Physics and Astronomy, University of Maryland, College Park, Maryland 20742

K. Aniol, M. B. Epstein, and D. J. Margaziotis

Department of Physics and Astronomy, California State University, Los Angeles, California 90032

J. M. Finn, C. Perdrisat, and V. Punjabi^{|||}

Department of Physics, College of William and Mary, Williamsburg, Virginia 23185

(Received 11 February 1998)

We measured the $^{12}\text{C}(e, e'p)$ cross section as a function of missing energy in parallel kinematics for $(q, \omega) = (970 \text{ MeV}/c, 330 \text{ MeV})$ and $(990 \text{ MeV}/c, 475 \text{ MeV})$. At $\omega = 475 \text{ MeV}$, at the maximum of the quasielastic peak, there is a large continuum ($E_m > 50 \text{ MeV}$) cross section extending out to the deepest missing energy measured, amounting to almost 50% of the measured cross section. The ratio of data to distorted-wave impulse approximation (DWIA) calculation is 0.4 for both p and s shells. At $\omega = 330 \text{ MeV}$, well below the maximum of the quasielastic peak, the continuum cross section is much smaller and the ratio of data to DWIA calculation is 0.85 for the p shell and 1.0 for the s shell. We infer that one or more mechanisms that increase with ω transform some of the single-nucleon knockouts into a multinucleon knockout, decreasing the valence knockout cross section and increasing the continuum cross section. [S0556-2813(99)00701-3]

PACS number(s): 25.30.Bf, 24.10.Eq, 25.30.Fj, 27.20.+n

I. INTRODUCTION

This paper reports a measurement of the quasielastic $^{12}\text{C}(e, e'p)$ reaction at momentum transfer $q \approx 1000 \text{ MeV}/c$ and two energy transfers $\omega = 330 \text{ MeV}$ and $\omega = 475 \text{ MeV}$. After an introductory discussion, we describe the experiment and its analysis. We present a representation of the differential cross section ω dependence around each of the two central values, using Legendre polynomials. Finally, we discuss the results of the experiment in terms of single-nucleon knockout, multinucleon knockout, and other processes. The Ph.D. thesis of Morrison [1] presents the experiment in more detail.

We define several quantities here: ω is the energy transferred from the electron to the nuclear system. The three-momentum transfer is \mathbf{q} , with magnitude q . The momentum transfer four-vector is $Q \equiv (\omega, \mathbf{q})$, and $Q^2 = q^2 - \omega^2$. The missing energy of the coincidence reaction is $E_m \equiv \omega - T_p$, where T_p is the outgoing proton kinetic energy. M is the mass of the nucleon. The missing momentum is $\mathbf{p}_m \equiv \mathbf{q} - \mathbf{p}_p$ where \mathbf{p}_p is the outgoing proton momentum.

At quasielastic kinematics $\omega \approx Q^2/2M$, interactions with independent nucleons are expected to dominate the nuclear electromagnetic response. However, despite the apparent agreement of nonrelativistic Fermi gas calculations [2] with

^{*}Present address: University of Houston Law Center, Houston, TX 77204.

[†]Present address: Department of Nuclear Medicine, UT MD Anderson Cancer Center, 1100 Holcombe Boulevard, Houston, TX 77030.

[‡]Present address: 9308 Cheney Hill Road, College Park, MD 20740.

[§]Present address: Department of Physics, Old Dominion University, Norfolk, VA 23529.

^{||}Present address: KVI, 9747 AA Groningen, The Netherlands.

[¶]Present address: SUNY at Stony Brook, Stony Brook, NY 11794-3800.

^{**}Present address: Department of Physics, Syracuse University, Syracuse, NY 13244.

^{††}Present address: I-Kinetics, Inc., 19 Bishop Allen Drive, Cambridge, MA 02139.

^{‡‡}Present address: 74 Boston Road, Apt. B-106, Chelmsford, MA 01824.

^{§§}Present address: USRA, Code 7654, Naval Research Laboratory, Washington, DC 20375-5352.

^{|||}Present address: Department of Physics, Norfolk State University, Norfolk, VA 23504.

quasielastic (e, e') measurements for a large range of nuclei [3], measurements of the separated longitudinal and transverse (e, e') cross sections have shown that other processes contribute significantly to the reaction. The longitudinal and transverse reduced response functions f_L and f_T for ${}^3\text{He}$ at $q \approx 500$ MeV/c [4] are equal, in accordance with the predictions of independent particle models. However, f_L is $\approx 40\%$ smaller than f_T for heavier nuclei including ${}^4\text{He}$, ${}^{12}\text{C}$, ${}^{40}\text{Ca}$, ${}^{56}\text{Fe}$, and ${}^{238}\text{U}$ [5–11] at $q \approx 500$ MeV/c. This indicates the presence of a nonquasifree process that may depend on the density or number of available nucleons.

Yates *et al.* [12] measured a different result on ${}^{40}\text{Ca}$: f_L is less than 20% smaller than f_T . At a larger momentum transfer $q = 1050$ MeV/c, f_L and f_T were comparable for both ${}^3\text{He}$ and ${}^4\text{He}$ on the low ω side of the quasielastic peak [13], but f_T was still significantly larger than f_L at $q = 1050$ MeV/c for ${}^{56}\text{Fe}$ [14]. Thus there is some experimental ambiguity in the magnitude and momentum-transfer dependence of the transverse-longitudinal (T - L) ratio.

Many different models of inclusive quasielastic electron scattering attempt to treat aspects of the reaction correctly, but no model can explain all of the data. Such older models include σ - ω calculations [15], meson-exchange currents [16], two-particle-two-hole models [17], modification of the mass and/or the size of the nucleon [18,19], and quark effects [20].

Recent Green's function Monte Carlo (GFMC) calculations by Carlson and Schiavilla [21], which include pion degrees of freedom, final state interactions, and two-body currents, can reproduce the ${}^3\text{He}$ and ${}^4\text{He}$ longitudinal and transverse response functions. They interpret the plane-wave impulse approximation (PWIA) response quenching as due to the charge-exchange component of the nuclear interaction, which shifts the strength to higher excitation energy. The quenching of the transverse response is more than offset by the contribution of two-body currents associated with pion exchange. This work indicates the necessity of including correlated initial state wave functions, two-body reaction mechanisms, and final state interactions. We expect that more reaction mechanisms, including real pions, deltas, and three-nucleon currents, need to be included for heavier nuclei and higher excitation energies. Unfortunately, no GFMC calculations are possible yet for heavier nuclei.

Coincidence ($e, e'p$) electron scattering, in which a knocked-out proton is detected in coincidence with the scattered electron, can distinguish among some of the various reaction processes proposed, because different reactions occur at different missing energies.

The $C(e, e'p)$ cross section was first measured at Saclay [22] out to $E_m \approx 60$ MeV and, more recently, by van der Steenhoven [23]. The spectrum exhibits a large narrow peak at $E_m \approx 16$ MeV, several small, narrow peaks at larger missing energies, and a broad structure from 25 MeV to 60 MeV. The momentum distributions indicated that the narrow peaks correspond to the knockout of a proton in a p -shell state, while the broad structure results from s -shell proton knockout. The spectroscopic factors were reported as 2.5 for the p -shell peaks and 1.0 for the s -shell peak [22]. The s -shell peak is broad because the residual nucleus is in an excited state and decays rapidly. Two-nucleon knockout may also contribute to the strength in the s -shell region as the thresh-

old for this process is at $E_m \approx 27$ MeV.

Lapikás [24] has found the strength for valence-shell knockout in ($e, e'p$) to be reduced by 20% for elements throughout the periodic table.

Several experiments at Bates have measured the $C(e, e'p)$ cross section as a function of missing energy for the following kinematical conditions: the maximum of the quasielastic peak at $q = 400$ MeV/c (an L/T separation), 585, 775, and 827 MeV/c [25,26]; the dip region at $q = 400$ MeV/c [27]; and the delta peak at $q = 400$ and 475 MeV/c [28]. These measurements had four major results.

(1) The cross section for single-nucleon ($e, e'p$) knockout is only 40%–60% of that predicted by distorted-wave impulse approximation (DWIA) analysis assuming four p -shell and two s -shell protons. This is consistent with the Saclay results and all other published quasielastic data. In the delta-region measurements, as expected, the single-nucleon knockout is virtually invisible.

(2) In stark contrast to the transverse response function, the longitudinal response function measured at $q = 400$ MeV/c is consistent with zero for $E_m \geq 50$ MeV. This suggests that single-nucleon knockout is minimal beyond $E_m = 50$ MeV.

(3) A considerable fraction of the cross section occurs at $E_m > 50$ MeV. The separated measurement at $q = 400$ MeV/c indicates that this strength is transverse and begins at $E_m \approx 27$ MeV, the threshold for two-nucleon emission. This “continuum” strength is attributed to two-nucleon and multinucleon knockout. The continuum strength persists in the measurements on the delta peak, and constitutes a large fraction of the total cross section even where pion production is expected to dominate. Note that excess transverse cross section was observed on other nuclei at missing energies above the two-nucleon emission threshold [29].

(4) No abrupt change in the cross section was seen at the pion threshold, $E_m \approx 155$ MeV, for $q = 775$ MeV/c, the only quasielastic measurement so far to probe sufficiently high missing energies. However, an abrupt increase in the cross section was seen in the delta-region measurements.

Figure 1 shows the momentum- and energy-transfer regions of the quasielastic, dip, and Δ measurements at Bates, including this experiment.

Kester *et al.* [31] have recently measured the ${}^{12}\text{C}(e, e'p)$ reaction in the dip region at a variety of angles away from parallel kinematics. They find that large-angle cross sections can be explained by meson-exchange currents and intermediate deltas, while smaller-angle cross sections suggest correlated pair emission.

II. EXPERIMENT

We report two measurements of the ${}^{12}\text{C}(e, e'p)$ reaction, at $q = 970$ and 990 MeV/c. Both were done in parallel kinematics. The energy transfers were respectively $\omega = 330$ and 475 MeV. The latter point is at the maximum of the $C(e, e')$ quasielastic peak, and extends the investigation of the momentum-transfer dependence of the $C(e, e'p)$ reaction cross section measured at $q = 400, 585, 775,$ and 827 MeV/c. With both measurements, we investigate how the single-nucleon and continuum cross sections depend on the energy

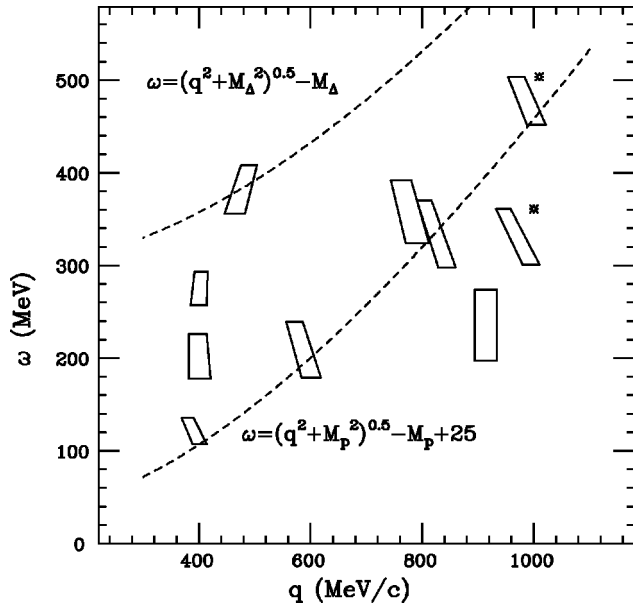


FIG. 1. The q and ω regions covered by the Bates $^{12}\text{C}(e,e'p)$ experiments [25–28,30]. The regions marked with an asterisk indicate the two measurements of this paper.

transfer on and below quasielastic kinematics. The specific kinematics are shown in Table I and Fig. 1.

We performed the experiment at the MIT-Bates Linear Accelerator Center in Middleton, MA. The recirculated electron beam had an average energy of $696 \text{ MeV} \pm 3 \text{ MeV}$ for the $\omega = 330 \text{ MeV}$ measurement and $796 \text{ MeV} \pm 3 \text{ MeV}$ for the $\omega = 475 \text{ MeV}$ measurement. The beam had a duty factor of approximately 1%, with 1–20 μA average (0.1–2 mA peak) current. We used several natural carbon targets with areal density or thickness ranging from 24 mg/cm^2 to 410 mg/cm^2 . We also used a spinning polyethylene target to measure the elastic $\text{H}(e,e')$ reaction for normalization, and tantalum and beryllium oxide targets for testing and calibration.

We used the magnetic spectrometers MEPS to detect electrons and OHIPS to detect protons. The polarity of OHIPS was reversed to detect electrons during calibration measurements. The spectrometers are described in detail elsewhere [1]. In each spectrometer, a scintillator array detected a particle passing through the spectrometer focal plane and triggered the readout system. A two-plane vertical drift chamber measured the particle trajectory at the focal plane. MEPS used an Aerogel Čerenkov counter with an index of refraction of 1.05 to distinguish between electrons and pions.

We identified coincidence events by the time elapsed between the electron trigger in MEPS and the proton trigger in OHIPS. The coincidence time resolution was approximately 2 ns full width at half maximum (FWHM). Accidental events

under the timing peak were subtracted, and this subtraction is included in the statistical errors of the spectra.

A. Calibrations, corrections, and efficiencies

We measured $\text{H}(e,e)$ in MEPS, elastic $\text{C}(e,e)$ in OHIPS, and coincidence $\text{H}(e,ep)$ at various spectrometer magnetic fields to determine the spectrometer constants and beam energies. The uncertainties are 3 MeV in the beam energy.

We calculated correction factors to account for losses due to many effects including software track reconstruction, simultaneous events in a wire chamber, more than one event per beam burst, and other software and hardware limitations. The correction factors varied from run to run, ranging from 1.40 to 1.90. Some correction factors were deduced from run-to-run variations and are only valid up to an overall normalization, discussed in the following section.

Because the (e,π^-p) cross section is much larger than the $(e,e'p)$ cross section at deep missing energies, we needed to reject pions. We used the $n = 1.05$ Aerogel Čerenkov counter in MEPS for this purpose. Electrons passing through the aerogel radiated Čerenkov light, whereas pions with momentum less than 430 MeV/c did not radiate. The electron detection efficiency of the Aerogel Čerenkov counter varied strongly with the MEPS magnetic field. For $\omega = 475 \text{ MeV}$, the electron detection efficiency was 93% and the pion rejection efficiency was 99.5%. For $\omega = 330 \text{ MeV}$, the electron detection efficiency was only 60% and the pion rejection efficiency was 98.5%. We also determined the electron detection efficiency as a function of focal plane position.

To obtain the relative acceptance (including detection efficiency) of the spectrometers as a function of focal plane position (i.e., of relative momentum), we measured the quasielastic $\text{C}(e,e')$ cross section in MEPS and the $\text{C}(e,p)$ cross section in OHIPS. We varied the magnetic field, placing particles with a given momentum at different positions in the focal plane. We deconvoluted the acceptance from the single-arm cross section to obtain the focal plane acceptance as a function of relative momentum. We then combined this with the variation in Čerenkov counter electron detection efficiency with focal plane position to get the total spectrometer relative efficiency-acceptance product (hereafter called “relative acceptance”). We applied these relative acceptances to all of our data. The absolute normalization of the spectrometers is discussed in the next section.

B. Normalizations

To normalize the experiment absolutely, we measured the $\text{H}(e,e')$ elastic cross section in MEPS, the $\text{H}(e,e'p)$ elastic cross section detecting electrons in MEPS and protons in OHIPS, and the $\text{C}(e,e')$ elastic cross section in OHIPS. We corrected these measured cross sections for the relative ac-

TABLE I. Experimental kinematics: Central values.

E_0 (MeV)	$ q $ (MeV/c)	ω (MeV)	$\Delta\omega$ (MeV)	θ_e (deg)	θ_p (deg)	p_m (<i>s</i> shell) (MeV/c)	p_m (<i>p</i> shell) (MeV/c)
696	970	330	65	129.7	17.0	−170.0	−144.0
796	990	475	60	118.1	17.0	19.0	43.0

ceptances as a function of momentum (described in the previous section). We then compared the corrected measured $H(e, e'p)$ cross section with the parametrization of Simon *et al.* of the $H(e, e')$ cross section [32] and the corrected $C(e, e')$ cross section with the phase-shift calculation of the program ELASTB [33].

Ideally, the $H(e, e'p)$ measurement would fully normalize the experiment after taking into account relative efficiencies and dead times. However, if the electron from $H(e, e'p)$ enters MEPS, kinematics restricts the proton to a small region within the OHIPS solid angle. $C(e, e'p)$ protons populate the entire OHIPS solid angle approximately uniformly. Particles entering OHIPS near the edges of the OHIPS collimator may not reach the focal plane. These losses affect the overall normalization, but $H(e, e'p)$ alone would not measure them.

We measured the elastic $C(e, e')$ cross section in OHIPS to account for those losses, but the electrons from $C(e, e')$ did not cover the OHIPS solid angle uniformly either. At 17° , the $C(e, e')$ cross section is approximately inversely proportional to the fourth power of the scattering angle. Most electrons entered OHIPS near the front of the angular acceptance.

We used the transport program TURTLE [34] to model the physical characteristics of OHIPS between the entrance near the target and the focal plane, and to estimate the fraction of particles entering the solid angle that reach the focal plane. We used three initial distributions of particles over the solid angle. TURTLE gave the following results for the indicated distribution of entering particles: (i) 100%, uniform over the restricted $H(e, e'p)$ region; (ii) 85%, inversely proportional to θ^4 as we expect for $C(e, e')$; (iii) 89%, uniform over the entire OHIPS solid angle as we expect for $C(e, e'p)$.

The $C(e, e')$ cross section measured in OHIPS was $(82 \pm 5)\%$ of the cross section calculated by ELASTB. After applying the correction functions calculated in the previous section for the Čerenkov counter inefficiency and the spectrometer acceptances as a function of momentum, the $H(e, e')$ and $H(e, e'p)$ measured cross sections were the same, indicating that OHIPS had no additional losses. The TURTLE results were consistent with both.

The overall normalization factor is the product of two terms: (i) The Mainz $H(e, e'p)$ cross section calculation divided by the measured $H(e, e'p)$ cross section, 1.06 for $\omega = 330$ MeV and 1.24 for $\omega = 475$ MeV, and (ii) The OHIPS factor from TURTLE and $C(e, e')$, given by $(1/0.89)[0.85/(0.82 \pm 0.05)] = 1.16 \pm 0.07$. The factor of $(1/0.89)$ comes from TURTLE for a uniformly illuminated solid angle. The factor $[0.85/(0.82 \pm 0.05)]$ is a small correction to the TURTLE normalization from the measured $C(e, e')$ cross section.

The normalization factors at the center of the focal plane (0% relative momentum) were 1.23 for $\omega = 330$ MeV and 1.44 for $\omega = 475$ MeV. Normalization factors at other locations on the focal plane were the product of the focal plane center normalization and the relative acceptance of the other location determined as described in the previous section.

The systematic uncertainty in the $C(e, e'p)$ cross section is 8% for the entire missing energy spectrum, primarily due to beam energy uncertainty coupled to the $C(e, e')$ and $H(e, e')$ cross sections and statistical uncertainty in the nor-

malization measurements. In addition, there is a further systematic uncertainty of 4% in the continuum region ($E_m > 50$ MeV) due to possible residual pion contamination.

C. Representation of the differential cross section

We measured the coincidence cross section as a function of missing energy for each of the two kinematics, at $\omega = 330$ MeV and 475 MeV, varying only the proton final momentum p_f . For each measurement, we represented the ω dependence of the cross section within the ω acceptance of the electron spectrometer by expanding the cross section around the central value of ω using orthogonal polynomials:

$$\frac{d^4\sigma}{d\Omega_e d\Omega_p d\omega dE_m} = \sum_{l=0}^{l_{\max}} \alpha_l(E_m) P_l\left(\frac{\omega - \omega_0}{\Delta\omega/2}\right), \quad (1)$$

where $P_l(x)$ are Legendre polynomials, ω_0 is the central value, and $\Delta\omega$ is the width of the ω acceptance. The experimental coefficients $\alpha_l(E_m)$ are determined from the data using the method described in [1]. For a given E_m , the true differential cross section is expected to vary smoothly with ω ; so $\alpha_l(E_m)$ should approach zero rapidly as l increases. This expansion of the ω dependence of the cross section is necessary since we lack sufficient experimental statistics to determine a full two-dimensional (E_m, ω) spectrum.

All α_l have the same units: pb/(MeV² sr²). Here $\alpha_0(E_m)$ is an average of the cross section over the ω acceptance. The nature of the average depends on the cutoff l_{\max} . Here $\alpha_1(E_m)$ multiplies $(\omega - \omega_0)/(\Delta\omega/2)$ in Eq. (1); it measures the change of the cross section over $\Delta\omega$. The ratio α_1/α_0 , which measures the relative change of the cross section with ω , may be more relevant in comparing the experiment with theory. Higher order terms (α_l with $l \geq 2$) multiply higher order polynomials of ω , and indicate the curvature of the cross section.

The calculation of the coefficients $\alpha_l(E_m)$ depends somewhat on the choice of cutoff l_{\max} . Values of α_l significantly different from zero are available from the data for $l=0, 1, 2$, and 3, although α_0 and α_1 yield the dominant features. We verified that α_l (for $l \leq l_{\max}$) was roughly independent of l_{\max} for $l_{\max}=2, 3$, or 4. Here α_0 calculated using $l_{\max}=0$ and using $l_{\max}=2, 3$, and 4 differ by less than 15%. For $l_{\max}=0$, α_0 is the average of the cross section over the ω acceptance. As l_{\max} increases, the variation of the cross section over the ω acceptance is described by the higher order terms so that α_0 becomes the cross section at the center of the ω acceptance.

The calculations we present use $l_{\max}=0$ and 3. The cross sections of the previous experiments at $q=400, 585$, and 775, and 827 MeV/ c were averaged over the ω acceptance, corresponding to α_0 with $l_{\max}=0$. Therefore, comparisons with previous measurements use the results from $l_{\max}=0$.

D. Radiative corrections

We used the prescription of Borie and Drechsel [35] to subtract the radiative tails of the p -shell and s -shell peaks from the missing energy spectra. Computing these tails requires knowledge of the coincidence cross section for all values of ω and E_m less than the experimental values. Lack-

ing this knowledge, we calculated both the peak and radiative tail cross sections using the PWIA and harmonic oscillator initial state wave functions. We scaled the tail calculation by the ratio of the measured peak cross section to the calculated peak cross section before subtracting the tail from the spectrum.

We calculated the Schwinger correction [36,37], with a hard photon cutoff of 11.5 MeV. We multiplied the p -shell peak by the Schwinger correction and subtracted the p -shell radiative tail from the s -shell and continuum regions of the spectrum. Then we multiplied the s -shell peak (limited to $E_m=50$ MeV) by the Schwinger correction using the same cutoff and subtracted the s -shell tail from the continuum region. Finally we applied the Schwinger correction to the continuum. We did not attempt to calculate continuum tails as we had no satisfactory model for them.

III. RESULTS AND DISCUSSION

A. Features of the spectra

Figures 2 and 3 show the Legendre expansion of the radiatively corrected cross section as a function of missing energy [$\alpha_0-\alpha_3$, calculated with $l_{\max}=3$ (see Sec. II C for a description of the expansion)]. (Note the difference in scales among the plots.) We see three features in α_0 for both kinematics: (i) a peak centered at $E_m=18$ MeV primarily due to single-nucleon knockout from the p shell, (ii) a broader peak out to $E_m\approx 60$ MeV primarily due to knockout from the s shell, but with a possible contribution from the continuum, and (iii) continuum strength at larger missing energy attributed to two-nucleon and multinucleon knockout. Ulmer's R_L/R_T separation at $q=400$ MeV/ c [25] indicates that s -shell knockout becomes small at 50 MeV and that the continuum strength starts at 27 MeV.

We note that the ratio of s -shell to p -shell cross sections is much smaller at $\omega=330$ MeV than at $\omega=475$ MeV. The continuum strength ($E_m>50$ MeV) extends beyond $E_m=300$ MeV for $\omega=475$ MeV, but goes to zero at approximately $E_m=90$ MeV for $\omega=330$ MeV. We do not see any increase in the cross section at the pion threshold, $E_m\approx 155$ MeV.

The $\omega=475$ MeV α_0 cross section spectrum appears to have a peak around $E_m=60$ MeV. The peak does not appear in the spectrum if we use a bin size of 6 MeV instead of the 3 MeV size used in Fig. 2, and we do not judge it statistically significant.

The α_1 spectra have features that correspond to the features of the α_0 spectra. In the $\omega=330$ spectrum, there is a narrow peak at 18 MeV and a broad peak beyond 25 MeV. These have corresponding peaks in the α_0 spectrum, and indicate that the cross section increases strongly across the ω acceptance. The continuum cross section beyond 50 MeV also has a large α_1 relative to α_0 , indicating that it also increases strongly with ω .

In the $\omega=475$ α_1 spectrum, the p -shell peak is small and positive, indicating a small average increase in the cross section over the ω acceptance. The s -shell α_1 is zero, indicating that the cross section is on the average constant over the ω acceptance. At 60 MeV of missing energy, α_1 becomes positive, suggesting that the reaction mechanism has changed. This is consistent with the result of the L - T separation at q

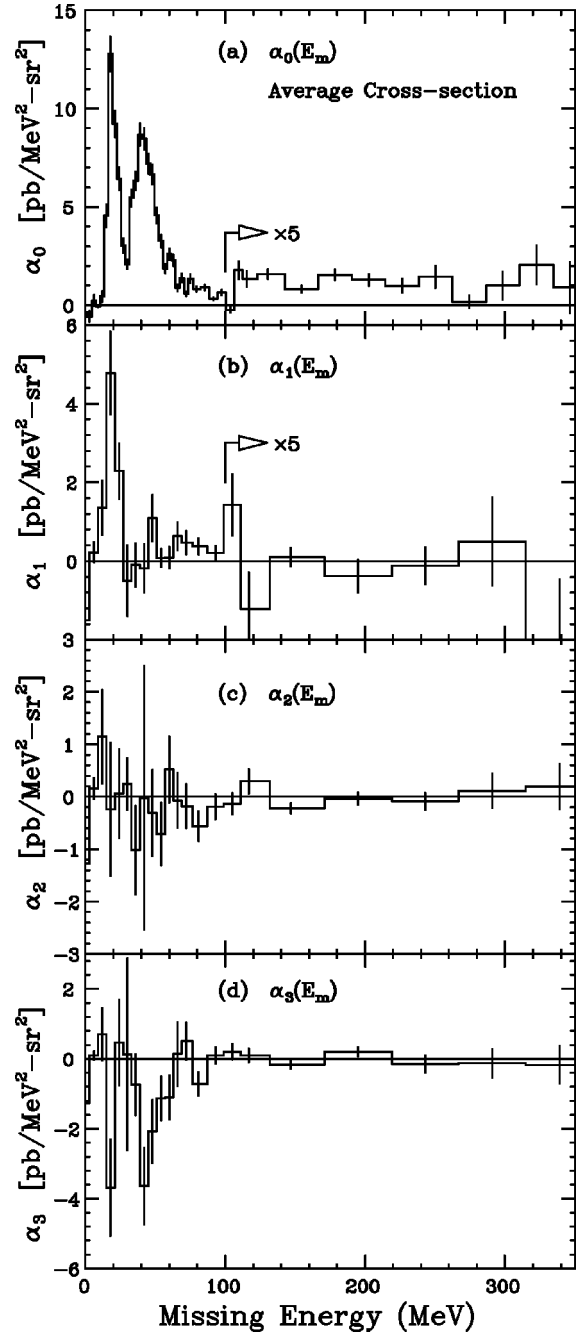


FIG. 2. Legendre expansion of the cross section vs missing energy for $\omega=475$ MeV. The quantities $\alpha_l(E_m)$ [with units $\text{pb}/(\text{MeV}^2 \text{sr}^2)$] are coefficients in the expansion of the cross section, Eq. (1). Here α_0 is an average of the cross section over ω ; α_1 is the linear change of the cross section over the ω acceptance. α_0 and α_1 have been multiplied by 5 for $E_m>100$ MeV for clarity. α_2 and α_3 are the second and third order changes in the cross section.

$=400$ MeV/ c [25] that s -shell single-nucleon knockout becomes small around 50 MeV. Beyond 110 MeV in missing energy, α_1 is consistent with zero, indicating no ω dependence within the acceptance.

Although α_0 and α_1 exhibit the most dominant and statistically significant features, α_2 and α_3 display some features. For $\omega=475$ MeV, α_2 is consistent with zero, but α_3 has a statistically significant negative value in the s -shell region and possibly in the p -shell region, indicating a mea-

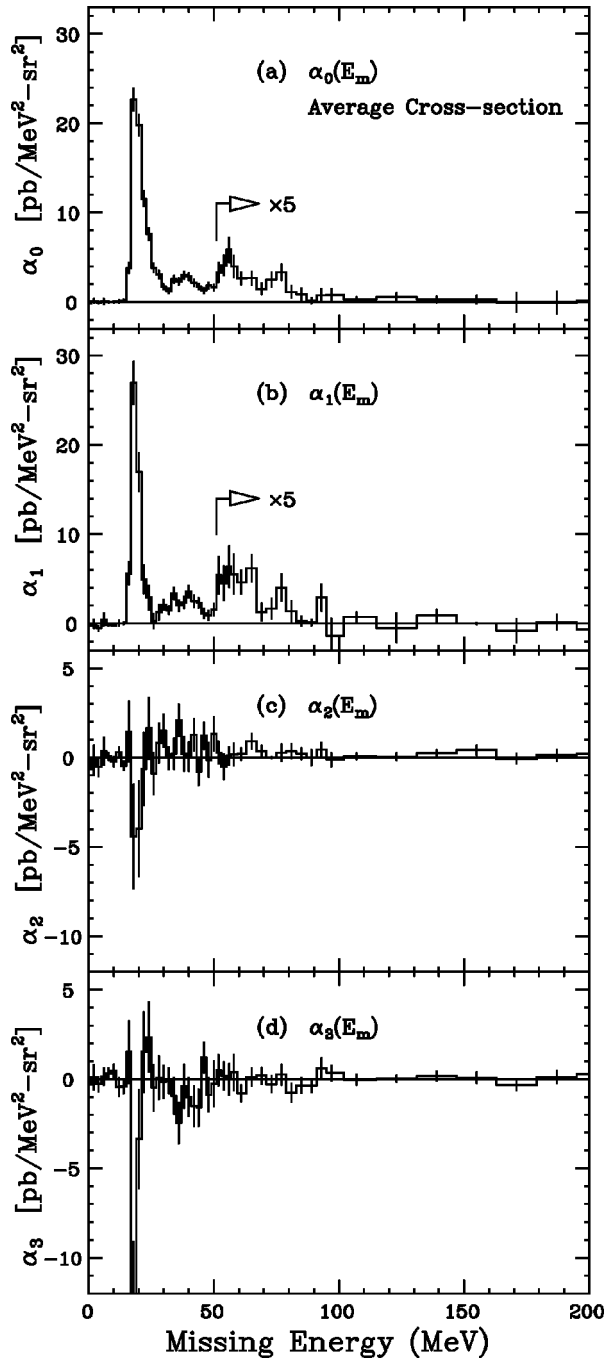


FIG. 3. Legendre expansion of the cross section vs missing energy for $\omega=330$ MeV. The quantities $\alpha_i(E_m)$ [with units $\text{pb}/(\text{MeV}^2 \text{sr}^2)$] are coefficients in the expansion of the cross section, Eq. (1). Here α_0 is an average of the cross section over ω ; α_1 is the linear change of the cross section over the ω acceptance. α_0 and α_1 have been multiplied by 5 for $E_m > 50$ MeV for clarity. α_2 and α_3 are the second and third order changes in the cross section.

surable curvature in the cross section as a function of ω . For $\omega=330$ MeV, α_2 and α_3 are consistent with zero except in the p -shell region, where they are both negative. We offer no interpretation of α_2 and α_3 in this paper.

B. Momentum distributions

The α_0 and α_1 spectra for the p and s shells collectively exhibit qualitative features consistent with the momentum

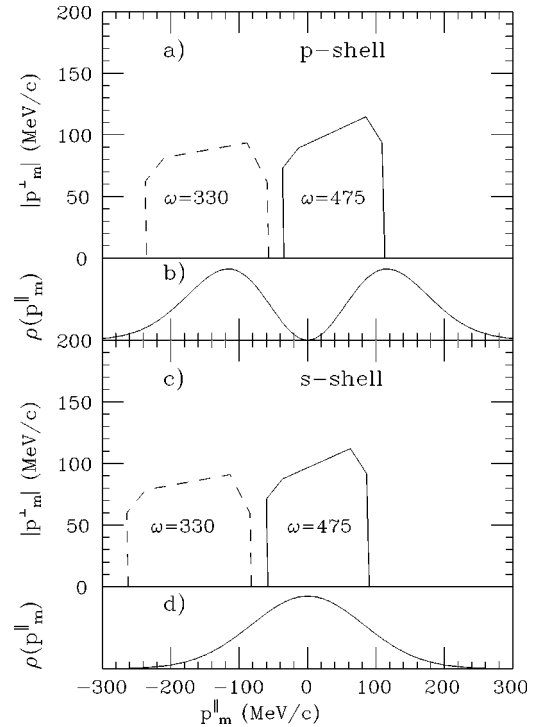


FIG. 4. Missing momentum acceptance of the experiment and schematic momentum distributions. (a) p -shell experimental acceptances (the magnitude of the perpendicular missing momentum $|\vec{p}_m^\perp|$ vs the parallel missing momentum p_m^\parallel) for the $\omega=475$ MeV and $\omega=330$ MeV measurements; (b) qualitative p -shell momentum distribution; (c) same as (a) for the s shell; (d) same as (b) for the s shell.

distributions expected of p - and s -shell orbitals, as displayed in Fig. 4. The s -shell momentum distribution has its maximum around zero missing momentum, while the p -shell momentum distribution has its maxima around ± 100 MeV/ c , and reaches a minimum at zero.

In parallel kinematics, the energy transfer is related to the missing momentum by

$$\omega - \frac{Q^2}{2M} \approx \frac{\mathbf{p} \cdot \mathbf{q}}{M} = \frac{p_m^\parallel q}{M}$$

for quasielastic single-nucleon knockout. Choosing ω determines the central value of the parallel component of the missing momentum. Although the experiment was centered at parallel kinematics, its finite angular and momentum acceptances covered a large range of the missing momentum perpendicular to \vec{q} . The parallel and perpendicular components of the missing momentum ranges sampled by the experiment are shown in Fig. 4. The central parallel missing momenta for the measurements are given in Table I. At $\omega=475$ MeV, the parallel component of the missing momentum covers approximately $-30 \text{ MeV} < p_m^\parallel < 100 \text{ MeV}$ (see Fig. 4). It is greater for the p shell than for the s shell, reflecting the difference in binding energy. The s -shell momentum distribution is near its maximum. Thus the s -shell

TABLE II. DWIA calculations for $\omega=330$ MeV. The data cross sections are integrated over the missing energy regions $E_m < 27$ MeV for the p shell and $27 \text{ MeV} < E_m < 50$ MeV for the s shell. The theory calculations are for one proton in the appropriate shell. The labels ‘‘Hama’’ [41] and ‘‘Meyer’’ [42] refer to the optical potentials used by the DWIA calculations. α_0 represents an average of the cross section over the ω acceptance. α_1 represents how the cross section increases over the acceptance. See text for details.

Shell		$l_{\max}=0$		$l_{\max}=3$	
		α_0 [pb/(MeV sr ²)]	α_0 [pb/(MeV sr ²)]	α_1 [pb/(MeV sr ²)]	α_1 / α_0
p shell	Data	$130 \pm 4 \pm 10$	$139 \pm 4 \pm 11$	116 ± 8	0.83 ± 0.09
	Hama	38.5 ± 4	40.4 ± 4	20.2 ± 2	0.50 ± 0.07
	Meyer	37.7 ± 4	40.2 ± 4	23.8 ± 2	0.59 ± 0.08
s shell	Data	$50.6 \pm 2 \pm 4$	$50.7 \pm 2 \pm 4$	49.3 ± 4	0.97 ± 0.12
	Hama	27.5 ± 4	27.3 ± 4	39.6 ± 6	1.5 ± 0.3
	Meyer	23.1 ± 4	22.9 ± 4	35.1 ± 6	1.5 ± 0.4

cross section should be flat in ω (i.e., α_1 should be small). The p -shell cross section should increase slightly with ω . We see these features in the α_0 and α_1 spectra in Fig. 2.

At $\omega=330$ MeV, the central parallel missing momentum is much larger than -100 MeV/ c . The p shell should dominate and both the p - and s -shell cross sections should increase strongly with ω . Here α_0 and α_1 in Fig. 3 reflect these traits. The p -shell cross section is much larger relative to the s -shell cross section at $\omega=330$ MeV than at $\omega=475$ MeV.

C. Distorted-wave impulse approximation

We compared the observed single-particle knockout strength from each shell with factorized DWIA cross section calculations. We integrated the observed cross section over missing energy from 10 MeV to 27 MeV for the p shell and from 27 MeV to 50 MeV for the s shell. The factorized DWIA cross section is given by

$$\frac{d^4\sigma}{d\Omega_e d\Omega_p d\omega dE_m} = E_f p_f \sigma_{ep} |\phi^D(\mathbf{p}_m, \mathbf{p}_f)|^2 f(E_m), \quad (2)$$

where σ_{ep} is deForest’s CC1 off-shell electron-proton cross section [38], $f(E_m)$ is the missing energy distribution for the shell, normalized to a unit area, and $|\phi^D(\mathbf{p}_m, \mathbf{p}_f)|^2$ is the effective distorted momentum distribution of the shell. We used a delta function for $f(E_m)$ to describe the p shell and a quadratic function between 30 and 50 MeV to describe the s shell.

Giusti and Pacati [39] have calculated the effects of Coulomb distortions of the electron wave function. They find effects of approximately 1%–2% for ^{12}C in parallel kinemat-

ics at an electron energy of 350 MeV. They also find that the effects decrease with initial energy. Since we performed this experiment at higher energies, we can disregard electron distortions.

We calculated $|\phi^D(\mathbf{p}_m, \mathbf{p}_f)|^2$ using the program PEEPSO, based on the nonrelativistic $(e, e'p)$ formalism of Boffi *et al.* [40]. PEEPSO converts the relativistic Dirac optical potential into a Schrödinger-equivalent potential including spin-orbit terms, and then solves the Schrödinger equation and calculates the unfactorized $(e, e'p)$ cross section for each shell, with a given separation energy, at the center of the spectrometer solid angle acceptances. The effective distorted momentum distribution is this calculated cross section divided by $E_f p_f \sigma_{ep}$. We used Woods-Saxon proton wave functions as measured by van der Steenhoven *et al.* at NIKHEF [23] for the initial bound states.

The optical potentials are fit to $C(p, p)$ elastic scattering results for different proton energies. We used the optical potential of Hama *et al.* [41] for the $\omega=475$ MeV measurement. For the $\omega=330$ MeV point, we calculated cross sections from the potential of Hama *et al.* and also from the parametrization of Meyer *et al.* [42]. The potential of Meyer *et al.* is only fit to $C(p, p)$ elastic scattering data for 200–300 MeV protons; we extrapolated it using the parametrized expressions.

We substituted the momentum distribution derived from PEEPSO into the factorized expression, Eq. (2), to obtain the cross section over the entire experimental solid angle and energy ranges. From this we derived theoretical predictions for $\alpha_1(E_m)$ as described in Sec. II C, averaged over the solid angle acceptances, using l_{\max} equal to 0 and 3 in Eq. (1).

Tables II and III display the results of the calculations

TABLE III. DWIA calculations for $\omega=475$ MeV. The data cross sections are integrated over the missing energy regions $E_m < 27$ MeV for the p shell and $27 \text{ MeV} < E_m < 50$ MeV for the s shell. The theory calculations are for one proton in the appropriate shell. α_0 represents an average of the cross section over the ω acceptance. α_1 represents how the cross section increases over the acceptance. See text for details.

Shell		$l_{\max}=0$		$l_{\max}=3$	
		α_0 [pb/(MeV sr ²)]	α_0 [pb/(MeV sr ²)]	α_1 [pb/(MeV sr ²)]	α_1 [pb/(MeV sr ²)]
p shell	Data	$92 \pm 3 \pm 7$	$100 \pm 4 \pm 8$	47 ± 8	
	theory	59.1 ± 7	70.1 ± 8	50.4 ± 6	
s shell	Data	$150 \pm 4 \pm 12$	$144 \pm 4 \pm 12$	0 ± 14	
	theory	182 ± 20	180 ± 20	-13.7 ± 20	

TABLE IV. Data-theory ratios. The data-theory ratios are the data cross sections divided by the DWIA cross sections from Tables II and III. For $\omega = 330$ MeV, the average of the calculations of Hama *et al.* and Meyer *et al.* was used.

	<i>p</i> shell		<i>s</i> shell	
	$l_{\max}=0$	$l_{\max}=3$	$l_{\max}=0$	$l_{\max}=3$
$\omega=330$ MeV	0.85 ± 0.11	0.86 ± 0.11	1.00 ± 0.18	1.01 ± 0.18
$\omega=475$ MeV	0.39 ± 0.06	0.36 ± 0.05	0.41 ± 0.06	0.40 ± 0.06

along with the data. The data differ from the calculations; the ratio is the “data-theory ratio.”¹ The potentials of Hama *et al.* and Meyer *et al.* give similar results for the $\omega=330$ MeV *p* shell, but less similar results for the *s* shell. We used the average of the two results for the calculated *s*-shell cross section, and assigned half the difference (10%) as an uncertainty in all the DWIA calculations due to the choice of potential. All other differences between the potentials of Hama *et al.* and Meyer *et al.* were less than 10%. We also calculated the DWIA cross sections using a delta-function *s*-shell distribution in missing energy. The difference between the delta-function *s*-shell result and the quadratic *s*-shell result was 10% for $\omega=330$ MeV and 3% for $\omega=475$ MeV. This contributed to the overall uncertainty in the *s*-shell DWIA calculations. We tested the factorization approximation by calculating the distorted momentum distribution [see Eq. (2)] from the PEEPSO unfactorized cross section at fixed (E_m, p_m) at the center and at the edges of the spectrometer angular acceptances. These differed by 5% for the $\omega=475$ MeV *p* shell and by 1% for the *s* shell and for both shells at $\omega=330$ MeV. The overall uncertainties were 15% for the $\omega=330$ *s*-shell calculation and 11% for the $\omega=330$ *p*-shell calculation, and both $\omega=475$ shells.

We obtained the “data-theory ratio” for each shell by dividing the measured cross section by the calculation. We used the average of the calculations of Hama *et al.* and Meyer *et al.* for the $\omega=330$ MeV theory cross section. The “data-theory ratios” calculated for $l_{\max}=0$ and 3 are given in Table IV. We use $l_{\max}=0$ to compare with results from prior papers. (See Sec. II C for a description of the Legendre expansion of the cross section.) Note that these comparisons of data to DWIA calculations are limited to the range of missing energies and missing momenta ($\Delta p_m \approx 200$ MeV/*c*) sampled by the measurements. No $(e, e'p)$ experiment has measured the entire three-dimensional missing momentum distribution.

At the quasielastic kinematics $\omega=475$ MeV, the data-theory ratios are 0.40 for both the *p* and *s* shells. Figure 5 shows these data-theory ratios, along with those from previous quasielastic and dip measurements. The data-theory ratios appear to be constant or perhaps decrease slightly with momentum transfer. The *s*-shell region ($27 < E_m < 50$ MeV) also includes two-nucleon knockout; this greatly increases the uncertainties of the *s*-shell data-theory ratios.

For $\omega=330$ MeV the data-theory ratios are 0.85 for the *p* shell and 1.0 for the *s*-shell, close to the naive expectation. The three-vector momentum transfer of 970 MeV is approximately the same as for $\omega=475$ MeV ($q=990$ MeV/*c*).

The *p*-shell data-theory ratio is approximately equal to the *s*-shell data-theory ratio for both data sets even though the ratio of *p*-shell cross section to *s*-shell cross section increases by factor of 4 between $\omega=475$ MeV and $\omega=330$ MeV. This lends credence to the model.

Ryckebusch has calculated $C(\gamma, N)$ and $C(e, e'p)$ differential cross sections from models that include two-nucleon knockout [43–45]. His single-nucleon knockout calculations include meson-exchange currents, delta currents, and Mahaux’s prescription for the missing energy spreading of the *s* shell. For the data presented in this paper, Ryckebusch’s *s*-shell knockout calculations match the above results; he ob-

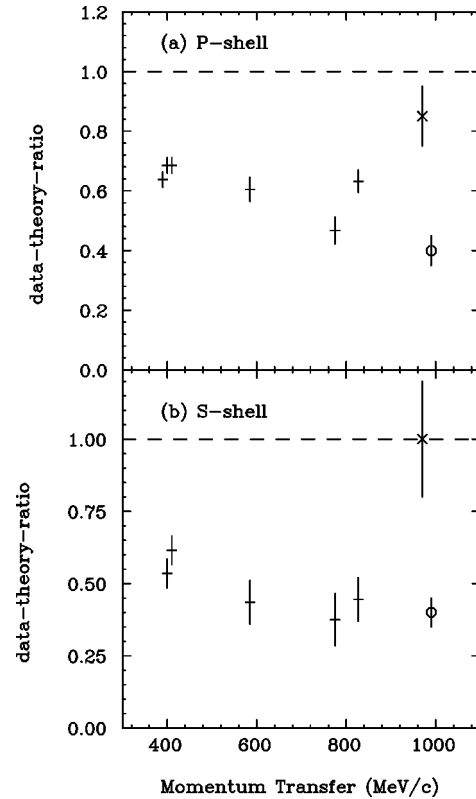


FIG. 5. The data-theory ratios from this and earlier experiments in the *p* shell (top plot) and the *s* shell (bottom plot) [25–28,30]. The data-theory ratio is given by the measured cross section integrated over the peak in missing energy, divided by the DWIA calculation. The $\omega=330$ MeV data-theory ratio for each shell is identified by an \times ; the $\omega=475$ MeV ratios are circles. Previously published spectroscopic factors are divided by the naive shell occupancy (*p* shell=4, *s* shell=2) to obtain data-theory ratios.

¹Other experiments refer to the “data-theory ratio” as a “spectroscopic factor” and use it to infer properties of the proton initial state wave function. The tremendous variation of the data-theory ratio with ω in this experiment casts doubt on the theory and precludes our using the term “spectroscopic factor.”

tains the same data-theory ratios of 1 for $\omega=330$ MeV and 0.4 for $\omega=475$ MeV. This also lends credence to the models.

This variation in data-theory ratios from quasielastic kinematics to low ω kinematics is qualitatively similar to that observed by van der Steenhoven *et al.* [23] who also measured a significantly larger ratio of data to DWIA at large negative missing momenta ($\omega \leq Q^2/2M$) than at positive missing momenta ($\omega \geq Q^2/2M$). Bernheim *et al.* [46] obtained a similar result.

The model of the $(e,e'p)$ cross section may have to be modified at large negative missing momentum. This is suggested from the measurement of α_1 at $\omega=330$ MeV in Table II. The ratio α_1/α_0 is 1.5 times theory for the p shell, indicating that the cross section is much steeper in ω or missing momentum than theory predicts. The reverse is true for the s shell.

Penn [30] has measured the $C(e,e'p)$ cross section for a similar momentum transfer, but a lower ω and larger p -shell central missing momentum: $\omega=235$ MeV and $|\mathbf{p}_m|=240$ MeV/ c . In Fig. 4, that would be farther to the left than the $\omega=330$ MeV measurement. Penn obtained a p -shell data-theory ratio of 0.45 ± 0.05 . This is similar to our $\omega=475$ MeV measurement, but different from $\omega=330$ MeV. However, the ratio α_1/α_0 at $\omega=330$ MeV is 1.5 times the DWIA calculation in Table II. Thus the experimental cross section decreases more rapidly with decreasing ω than theory predicts, leading us to expect a lower data-theory ratio at lower ω using the same model.

We recognize limitations in the available DWIA models. In particular, variations due to different optical potentials are already included in our estimate of the uncertainty of the data-theory ratios. In addition, the code PEEPSO does not include relativistic dynamics. However, the factor of 2 difference between the $\omega=330$ MeV and the $\omega=475$ MeV data-theory ratios remains a challenge for nuclear theory.

D. Quasielastic $C(e,e')$ cross section

We have also measured the single-arm quasielastic $^{12}\text{C}(e,e')$ cross section for each energy transfer. We used a model by Warren and Weinstein [47] to extrapolate the measured coincidence single-proton-knockout cross section of each shell to the entire 4π sr nucleon solid angle. We compared the sum of the p - and s -shell extrapolations with the measured single-arm cross section. For $\omega=330$ MeV, the extrapolated coincidence cross section was 0.93 ± 0.04 of the single-arm cross section. For $\omega=475$ MeV, the extrapolated coincidence cross section was 0.50 ± 0.05 of the single-arm cross section. These ratios are consistent with the $C(e,e'p)$ data-theory ratios.

E. Multinucleon knockout and other processes

In Fig. 2, we see extensive cross section beyond $E_m=50$ MeV at quasielastic kinematics ($\omega=475$ MeV). This strength is approximately constant beyond about 100 MeV, and appears to extend out to the deepest missing energy measured. The strength is similar to that seen in previous quasielastic measurements [25–27]. Below the quasielastic peak, at $\omega=330$ MeV, the continuum strength is present, but far weaker relative to the single-nucleon cross section, and is consistent with zero beyond $E_m=90$ MeV. We plot the ratio

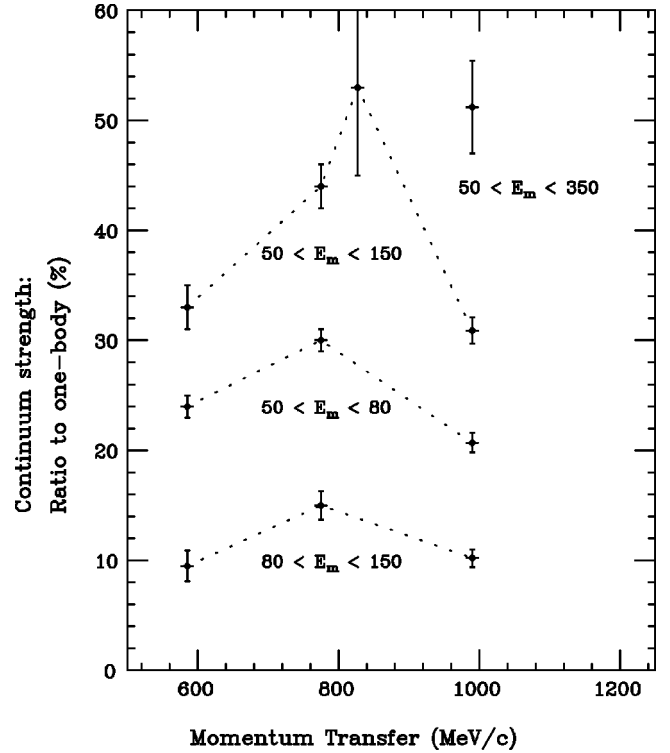


FIG. 6. The ratio of multinucleon knockout ($E_m > 50$ MeV) to single-nucleon knockout ($E_m < 50$ MeV) for this experiment ($\omega = 475$ MeV) and earlier experiments [25–28,30].

of the multinucleon-knockout cross section (integrated over $E_m > 50$ MeV) to the single-nucleon-knockout cross section (integrated over $E_m < 50$ MeV) for various continuum regions from previous experiments and the $\omega=475$ MeV measurement in Fig. 6.

We estimated the contribution of multistep processes, such as $(e,e'N)$ followed by (N,p) , to the continuum cross section, by convoluting the PWIA nucleon-knockout reaction with two models of (N,p) scattering. The first model uses the intranuclear cascade code MECC-7 [48] to conduct a Monte Carlo simulation of the propagation of nucleons through the nucleus as a series of independent collisions with other nucleons. The code enforces the Pauli exclusion principle in the collisions. The second model uses $C(p,p')$ data at 300 MeV and 20° , and at 500 MeV and 16° [49]. We multiplied the results from the $C(p,p')$ data by 1.5 to approximately include neutrons, because the $(e,e'N)$ cross section is approximately proportional to the square of the magnetic moment, and $(\mu_n/\mu_p)^2 \approx 0.5$. The results are given in Table V, along with the measured cross sections from this experiment. These calculations can only account for less than 6% of the data beyond $E_m=27$ MeV. The MECC-7 calculation produces almost no cross section beyond $E_m=100$ MeV. The $C(p,p')$ -based calculation reaches its maximum at $E_m=70$ – 80 MeV, but has a long tail reaching to the deepest missing energy. Half its cross section may lie beyond $E_m=100$ MeV.

The cross section out to 90 MeV in missing energy in both $\omega=330$ and $\omega=475$ MeV measurements has the approximate shape expected from Takaki's model of two-nucleon knockout [50]. However, its magnitude is larger by a factor of 16 [51]. Beyond 90 MeV, the shape at $\omega=475$

TABLE V. Multiple-scattering cross sections. The measured cross sections, integrated over the given regions, are compared with rescattering calculations convoluting $(e, e'N)$ with (N, p) cross sections based on MECC-7 calculations [48] and $C(p, p')$ data [49]. The $C(p, p')$ cross sections results were multiplied by 1.5 to approximately account for initial neutron interactions.

	$\omega = 330$ MeV	$\omega = 475$ MeV
Multiple scattering with MECC-7	2.4 pb/(MeV sr ²)	9.6 (pb/MeV sr ²)
Multiple scattering with $C(p, p')$ data $\times 1.5$	4.4	15.6
Data, s shell $C(e, e'p)(E_m = 27\text{--}50$ MeV)	51 ± 2	150 ± 4
Data, near continuum $C(e, e'p)(E_m = 50\text{--}100$ MeV)	23 ± 2	68 ± 3
Data, full continuum $C(e, e'p)(E_m = 50\text{--}350$ MeV)	23 ± 2	130 ± 10

MeV is consistent with Takaki's three-nucleon-knockout model. At $\omega = 330$ MeV, there is no strength beyond 90 MeV; the continuum strength up to 90 MeV should be mostly due to two-nucleon knockout.

Both rescattering calculations [MECC-7 and $C(p, p')$] and Takaki's calculation used harmonic oscillator initial state momentum distributions. It is unlikely that using bound states derived from realistic Woods-Saxon potentials will change this result at $\omega = 475$ MeV where the initial momenta involved are small. Even at $\omega = 330$ MeV, the initial momenta of 100–250 MeV/ c are reasonably small. In addition, the strong decrease of the continuum cross section at large E_m for $\omega = 330$ MeV compared to $\omega = 475$ MeV indicates that an initial momentum distribution plus rescattering cannot explain the continuum cross sections. However, initial state correlations could contribute to the cross section at deep missing energy, because two nucleons share the transferred energy and we detect only one nucleon. The $C(p, p')$ rescattering calculation shows a larger tail than the MECC-7 calculation; this may reflect such correlations. If so, those correlations are not strong enough to explain our continuum cross section when they are part of the rescattering picture.

However, neither the $C(p, p')$ nor MECC-7 calculations included such correlations in the initial $(e, e'N)$ reaction; the initial nucleon bound state was a simple harmonic oscillator. If the large yield we see at deep missing energy results from strong initial state correlations, this is very interesting. But this is unlikely to explain the longitudinal response at $q = 400$ MeV/ c [25] which is small beyond $E_m = 50$ MeV. The dynamical correlations should influence both the longitudinal and transverse responses.

Later in Sec. III F of this paper (Fig. 7), we discuss calculations by Ryckebusch using initial state Jastrow correlations. Ryckebusch was unable to generate more than 1% of our $\omega = 475$ MeV continuum cross section from the correlations. Furthermore, one could use Ryckebusch's missing energy spectrum as an input to a rescattering calculation. Ryckebusch's calculated s shell (which does not include correlations) fits our data after renormalization for data-theory ratios; it should therefore generate a rescattering cross section comparable to our estimates. Ryckebusch's continuum cross section (which includes correlations) is 10^{-3} of his s -shell cross section and 10^{-2} of our measured continuum cross section. Thus, his continuum cross section cannot generate through rescattering a cross section comparable to our data.

We see no increase in strength at the pion threshold, $E_m \approx 155$ MeV. Baghaei's PWIA Δ -resonance pion-production

calculation [28,53] predicts more strength than we see beyond the pion threshold. A calculation that we performed based on Nozawa and Lee's pion-production model [52] involving both nonresonant and resonant production underpredicts the cross section in that region by about half. The calculation also predicts the pion-production cross section to increase with ω , resulting in a positive α_1 . Basic considerations of pion production occurring at the tail of the Δ resonance also lead to the same conclusion. The measured α_1 and the ratio α_1/α_0 are consistent with zero and inconsistent with the pion-production prediction. The results of the pion-production calculations are presented in Table VI.

We estimate an upper bound on the amount of two-nucleon knockout due to N - Δ interactions. Pion scattering

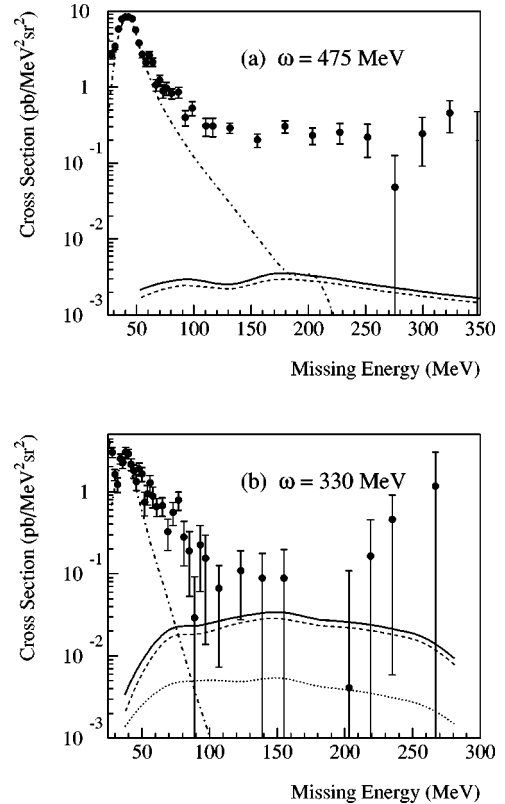


FIG. 7. Cross sections calculated by Ryckebusch [45]. The points are the measured cross section ($l_{\max} = 0$), the dot-dashed line is single-nucleon knockout from the s shell, the dotted line (too small to see in $\omega = 475$ MeV) is from $(e, e'pp)$; the dashed line is from $(e, e'pn)$, and the solid line is the total multinucleon-knockout cross section. The cross section is displayed for $E_m > 25$ MeV, omitting the p shell.

TABLE VI. Pion-production calculations. The data are the $\omega=475$ MeV calculation integrated over the $E_m>155$ MeV, pion threshold. Pion-production calculations are based on Baghaei [53] and Nozawa and Lee [52].

	α_0	α_1	α_1/α_0
Data	29.2 ± 3.8	-4.3 ± 6.2	-0.15 ± 0.21
Baghaei (Δ)	45.3		
Nozawa and Lee (Born+ Δ)	13.0	11.5	0.88

experiments indicate that the two-nucleon-knockout cross section from the reaction $N\Delta \rightarrow 2N$ is comparable to the pion-nucleon-production cross section due to $\Delta \rightarrow N\pi$ [54]. The latter has to be less than the total integrated cross section above $E_m = 155$ MeV. In the $\omega=475$ MeV measurement, if we assume that the cross section for $N\Delta \rightarrow NN$ is less than or equal to the integral of the experimental cross section for $E_m > 155$ MeV and we distribute this strength in missing energy according to Takaki's shape for two-nucleon knockout in the region $50 < E_m < 150$ MeV, then $\Delta N \rightarrow NN$ can account for at most one-sixth of the cross section for $50 < E_m < 100$ MeV and none of the cross section above 100 MeV. At $\omega=330$ MeV, this can account for none of the cross section. However, one must be cautious; at quasielastic kinematics, many of the Δ 's may not have enough mass to decay into a real pion and a real nucleon. The two-nucleon cross section due to $N\Delta$ interactions could be greater than the above estimate.

F. Recent multinucleon calculations

Ryckebusch has calculated $C(\gamma, N)$ and $C(e, e'p)$ differential cross sections from models that include two-nucleon knockout [43–45]. His single-nucleon-knockout calculations include meson-exchange currents, delta currents, and Mahaux's prescription for the missing energy spreading of the s shell. His two-nucleon-knockout cross sections include Jastrow correlations in addition.

These calculations fit the shape of the single-nucleon-knockout part of our data. Using Mahaux's s -shell spreading, these calculations also fit our data out to $E_m \approx 60$ MeV. This is consistent with the experiment reported by Makins [55] at $Q^2 = 1$ (GeV/c)². Their calculations appear to match their data using only single-nucleon-knockout and radiative corrections, but their cross section data extend only out to $E_m = 100$ MeV. (Note that in this paper we use $E_m = 50$ MeV as the starting point for multinucleon knockout since R_L is small beyond that point.)

Ryckebusch's calculations of real photon absorption understate the measured $C(\gamma, N)$ cross sections at forward angles and at high missing energies by about half [43,44]. His preliminary $C(e, e'p)$ calculations [45] also account for at most half the cross section beyond $E_m = 70$ MeV measured in parallel kinematics at Bates for $q = 585$ MeV/c, $\omega = 210$ MeV. However, his calculations reproduce data taken in nonparallel kinematics at NIKHEF [30] far from quasielastic kinematics— $q = 270$ MeV/c, $\omega = 212$ MeV, and $\theta_{pq} = 42^\circ$.

For the data presented in this paper, Ryckebusch's calculated multinucleon-knockout cross section is less than 1% of the measured continuum cross section at $\omega=475$ MeV (see Fig. 7). For $\omega=330$ MeV, well below quasielastic kinematics, his calculations are consistent with the measurement beyond $E_m = 100$ MeV, although the measurement is also consistent with zero. Ryckebusch predicts more multinucleon knockout at $\omega=330$ MeV than at $\omega=475$ MeV; we see the opposite effect.

Recently Benhar [56] calculated the continuum cross sections at $E_m > 220$ using a correlated nuclear matter spectral function in the PWIA. The magnitude of his calculated cross sections is consistent with the data at $\omega=475$ MeV and slightly overpredicts the data at $\omega=330$ MeV. However, his calculated cross section decreases much more rapidly with missing energy than do the data. A calculation using the ^{12}C spectral function would be very valuable to help us understand the large differences between the $\omega=330$ and 475 MeV measurements in both the valence-knockout and continuum regions.

IV. CONCLUSIONS

The different data-theory ratios at $\omega=330$ MeV and at $\omega=475$ MeV are consistent with the different cross sections seen beyond $E_m=50$ MeV. At $\omega=330$ MeV, we see nearly four p -shell and two s -shell protons, but little continuum cross section. At $\omega=475$ MeV, we see half as many protons, but much more continuum cross section, extending out to the deepest missing energy measured (Figs. 2 and 6). We associate the cross section at $E_m > 50$ MeV with multinucleon knockout. We infer that some mechanism that increases with ω transforms some of the single-nucleon knockout into multinucleon knockout.

The measurement at $\omega=475$ MeV strongly confirms prior results that the (e, e') reaction at quasielastic kinematics involves strong many-body physics and reactions in addition to quasielastic knockout. These other reactions do not stem from either nucleon rescattering or from Δ interactions.

The $\omega=330$ MeV measurement indicates that well below quasielastic kinematics, but above collective phenomena such as giant resonances, the (e, e') reaction is primarily single-nucleon quasielastic knockout. The data-theory ratios, within large uncertainties, are close to the expected values from the simple shell model. However, there is still some residual many-body physics at that low energy transfer.

These data, especially the strength at high missing energies, strongly support the growing realization that the inclu-

sive (e, e') quasielastic peak contains much more many-body physics than was originally thought. This additional complexity persists at large momentum transfer and is not understood. The low ω side of the quasielastic peak appears to be dominated by the simple single-nucleon-knockout pro-

cess, but some complexity still appears.

This work was supported in part by the Department of Energy under Contract No. DE-AC02-76ERO3069 and the National Science Foundation.

-
- [1] J. Morrison, Ph.D. thesis, MIT, 1993.
- [2] E. Moniz, I. Sick, R. Whitney, J. Ficenece, R. Kephart, and W. Trower, *Phys. Rev. Lett.* **26**, 445 (1971).
- [3] B. Whitney, I. Sick, J. Ficenece, R. Kephart, and W. Trower, *Phys. Rev. C* **9**, 2230 (1974).
- [4] C. Marchand *et al.*, *Phys. Lett.* **153B**, 29 (1985).
- [5] K. von Reden *et al.*, *Phys. Rev. C* **41**, 1084 (1990).
- [6] R. Altemus *et al.*, *Phys. Rev. Lett.* **44**, 965 (1980).
- [7] J. M. Finn *et al.*, *Phys. Rev. C* **29**, 2230 (1984).
- [8] Z. E. Meziani *et al.*, *Nucl. Phys.* **A446**, 113 (1985).
- [9] Z. E. Meziani *et al.*, *Phys. Rev. Lett.* **52**, 2130 (1984).
- [10] P. Barreau *et al.*, *Nucl. Phys.* **A402**, 515 (1983).
- [11] C. C. Blatchley *et al.*, *Phys. Rev. C* **34**, 1243 (1986).
- [12] T. C. Yates *et al.*, *Phys. Lett. B* **312**, 382 (1993).
- [13] Z. E. Meziani *et al.*, *Phys. Rev. Lett.* **69**, 41 (1992).
- [14] J.P. Chen *et al.*, *Phys. Rev. Lett.* **66**, 1283 (1991).
- [15] B. Serot and J. Walecka, in *Advances in Nuclear Physics*, edited by J. W. Negele and E. Vogt (Plenum Press, New York, 1986), Vol. 16.
- [16] J. W. van Orden and T. W. Donnelly, *Ann. Phys. (N.Y.)* **131**, 451 (1981).
- [17] W. Alberico *et al.*, *Ann. Phys. (N.Y.)* **154**, 356 (1984).
- [18] J.V. Noble, *Phys. Rev. Lett.* **46**, 412 (1981).
- [19] L.S. Celenza *et al.*, *Phys. Rev. C* **33**, 1012 (1986).
- [20] P.J. Mulders, *Nucl. Phys.* **A459**, 525 (1986).
- [21] J. Carlson and R. Schiavilla, *Phys. Rev. C* **49**, R2880 (1994); (private communication).
- [22] J. Mougey *et al.*, *Nucl. Phys.* **A262**, 461 (1976).
- [23] G. van der Steenhoven *et al.*, *Nucl. Phys.* **A480**, 547 (1988).
- [24] L. Lapikás, *Nucl. Phys.* **A553**, 297c (1993).
- [25] P. E. Ulmer *et al.*, *Phys. Rev. Lett.* **59**, 2259 (1987).
- [26] L. B. Weinstein *et al.*, *Phys. Rev. Lett.* **64**, 1646 (1990).
- [27] R. W. Lourie *et al.*, *Phys. Rev. Lett.* **56**, 2364 (1986).
- [28] H. Baghaei *et al.*, *Phys. Rev. C* **39**, 177 (1989).
- [29] J. B. J. M. Lanen *et al.*, *Phys. Rev. Lett.* **64**, 2250 (1990).
- [30] S. Penn, Ph.D. Thesis, MIT, 1993.
- [31] L. J. H. M. Kester *et al.*, *Phys. Lett. B* **344**, 79 (1995).
- [32] G. G. Simon *et al.*, *Nucl. Phys.* **A333**, 381 (1980).
- [33] B. Norum *et al.* (private communication).
- [34] D. C. Carey, K. L. Brown, and C. H. Iselin, "DECAY TURTLE, A Computer Program for Simulating Charged Particle Beam Transport System, Including Decay Calculations," Report No. SLAC-246, UC-28 (1/A), 1982.
- [35] E. Borie and D. Drechsel, *Nucl. Phys.* **A167**, 369 (1971).
- [36] J. Schwinger, *Phys. Rev.* **76**, 790 (1949).
- [37] L. Maximon, *Rev. Mod. Phys.* **41**, 193 (1969).
- [38] T. deForest, *Nucl. Phys.* **A392**, 232 (1983).
- [39] C. Giusti and F. Pacati, *Nucl. Phys.* **A473**, 717 (1987).
- [40] S. Boffi *et al.*, *Nucl. Phys.* **A336**, 437 (1980).
- [41] S. Hama, B. C. Clark, E. D. Cooper, and R. L. Mercer (private communication).
- [42] H.-O. Meyer *et al.*, *Phys. Rev. C* **37**, 544 (1988).
- [43] J. Ryckebusch *et al.*, *Nucl. Phys.* **A568**, 828 (1994).
- [44] J. Ryckebusch *et al.*, *Phys. Rev. C* **49**, 2704 (1994).
- [45] J. Ryckebusch (private communication).
- [46] M. Bernheim *et al.*, *Nucl. Phys.* **A375**, 381 (1982).
- [47] L. B. Weinstein and G. Warren, *Phys. Rev. C* **50**, 350 (1994); and (private communication).
- [48] "MECC-7, Medium Energy Intra-nuclear Cascade Code," Oak Ridge National Laboratory Report No. CCC-156, 1971.
- [49] R. Segal (private communication).
- [50] T. Takaki, *Phys. Rev. Lett.* **62**, 395 (1989).
- [51] T. Takaki, *Phys. Rev. C* **39**, 359 (1989).
- [52] S. Nozawa and T.-S. H. Lee, *Nucl. Phys.* **A513**, 511 (1990).
- [53] H. Baghaei, Ph.D. thesis, MIT, 1987.
- [54] D. Ashery *et al.*, *Phys. Rev. C* **23**, 2173 (1981).
- [55] N. C. R. Makins, Ph.D. thesis, MIT, 1994; N. C. R. Makins *et al.*, *Phys. Rev. Lett.* **72**, 1986 (1994).
- [56] O. Benhar (private communication); O. Benhar *et al.*, *Nucl. Phys.* **A505**, 267 (1989).